

Article

Optimisation of Control Algorithm for Hydraulic Power Take-Off System in Wave Energy Converter

Niklas Enoch Andersen ¹, Jakob Blåbjerg Mathiasen ¹, Maja Grankær Carøe ¹ , Chen Chen ¹,
Christian-Emil Helver ¹, Allan Lynggaard Ludvigsen ¹ , Nis Frededal Ebsen ² 
and Anders Hedegaard Hansen ^{1,*} 

¹ AAU Energy, Aalborg University, 9220 Aalborg, Denmark

² Floating Power Plant A/S, 4941 Bandholm, Denmark

* Correspondence: ahh@energy.aau.dk

Abstract: Wave energy converters are still a maturing technology and, as such, still face a series of challenges before they can compete with already-established technologies. One of these challenges is optimising the amount of energy extracted from the waves and delivered to the power grid. This study investigates the possibility of increasing the energy output of the existing hydraulic power take-off system of a wave energy converter made by Floating Power Plant during small-scale testing of their hybrid wind and wave energy platform. This system consists of a floater arm that rotates an axle when displaced by the waves. When the axle rotates, two hydraulic cylinders are actuated, displacing oil to run through a hydraulic motor driving an electric generator. The energy extraction is controlled by implementing a control algorithm on a series of on/off valves, which decouples the two hydraulic cylinders driving the hydraulic motor, and by varying the applied torque from the generator to match the wave conditions. Finally, it is investigated whether adding high-pressure pathways to the cylinder pressure chambers is beneficial for maximum power point tracking with reactive control. The analysis is conducted through a numerical model developed in Simulink and verified by comparison to the experimental setup supplied by Floating Power Plant. The study finds that a continuous valve switching strategy is optimal compared to end-point switching and reactive control with high-pressure pathways.

Keywords: power take-off; wave energy; fluid power; hydraulics; wave power extraction algorithm; numerical simulation; experimental testing



Citation: Andersen, N.E.; Mathiasen, J.B.; Carøe, M.G.; Chen, C.; Helver, C.-E.; Ludvigsen, A.L.; Ebsen, N.F.; Hansen, A.H. Optimisation of Control Algorithm for Hydraulic Power Take-Off System in Wave Energy Converter. *Energies* **2022**, *15*, 7084. <https://doi.org/10.3390/en15197084>

Academic Editor: Mário José Gonçalves Cavaco Mendes

Received: 6 July 2022

Accepted: 16 September 2022

Published: 27 September 2022

Publisher's Note: MDPI stays neutral with regard to jurisdictional claims in published maps and institutional affiliations.



Copyright: © 2022 by the authors. Licensee MDPI, Basel, Switzerland. This article is an open access article distributed under the terms and conditions of the Creative Commons Attribution (CC BY) license (<https://creativecommons.org/licenses/by/4.0/>).

1. Introduction

Wave energy has great potential to be a large contributor to the global energy market. Studies have shown a high energy potential in harvesting energy from ocean waves and set the global theoretical potential as high as 32.000 TWh/year [1]. Harvesting wave energy can be done in various ways, from taking advantage of the tidal waves close to the shore to placing a stationary platform out on the sea to harvest the wave energy of the ocean [2]. A thorough review of wave energy technologies is beyond the scope of this paper, but interested readers can consult papers such as [3].

Wave energy technologies face various challenges where the harsh sea environments put high demands on the construction being able to withstand continuous water exposure, high waves, strong currents, and winds. One of the main challenges is, that wave energy technologies must be able to harvest energy continuously despite waves changing in amplitude and frequency. Varying waves put a high demand on Power Take-Off (PTO) technology because fluctuating weather and waves place a high demand on agile energy harvesting solutions [4]. Fluid power technologies has largely been found applicable as PTO systems in wave energy converters, see, e.g., [5] for a review of fluid power PTO systems.

Floating Power Plants (FPP) combine wind and wave energy on a floating platform featuring a wind turbine and four wave absorbers. Each wave absorber drives a hydraulic PTO system. The FPP power take-off system utilises a Discrete Displacement Cylinder (DDC) technology combined with a fixed displacement hydraulic motor driving an electrical generator. This study investigates control algorithms for a hydraulic PTO system. Only a few other wave energy converter technologies have utilised active discrete fluid power PTO systems. In [6] a discrete fluid power PTO system is investigated and shows promising potential; however, this system enables bi-directional power flow, whereas the FPP system only supports uni-directional power flow. In [7], advanced control of the DDC system of [6] is investigated, and it was found that predictive control with proper wave model for cast may improve energy harvesting.

The hydraulic PTO system may be controlled in various ways by opening and closing valves in the DDC part of the system and by varying the counter torque exerted by the generator through a frequency converter. The control algorithms for the PTO system, called wave power extraction algorithms (WPEA), aim to maximise the energy output to the grid.

There are different methods of categorising different approaches to WPEAs, one of which is categorising them based on power flow direction. When the power flow is bidirectional, the PTO system can affect the absorber's motion by applying a force in the same direction as the wave motion, enhancing the oscillating motion, and maximising the mechanical energy. This type of WPEA is categorised as reactive control.

The second type of control is resistive control. Here, the power flow is unidirectional, and the PTO system can only extract energy from the absorber motion by applying force opposing absorber movement. Compared to reactive control, this strategy will usually cause a lower mechanical energy absorption. However, it does not mean that the final energy production is always higher for reactive control compared to resistive control, when the conversion losses are considered. The PTO system from Floating Power Plant (FPP) is currently designed to operate with resistive control strategies.

In [4], it is found that using reactive control to increase power absorption, at the time, had questionable feasibility, but proves that reactive control is beneficial for various PTO systems. Furthermore, ref. [8] states that reactive control is being improved in terms of its reliability, survivability, effectiveness, and ability to harvest energy. In other words, reactive control still has room for improvement in various areas before nearing the point of commercialisation.

The primary purpose of this study is to improve the WPEA for FPP by exploring different control strategies within the subject of resistive control. In addition, it will be investigated whether an increase in generated power is achieved if the system is modified such that a reactive control approach can be realised. This study will, hence, investigate how to design a WPEA for this novel PTO structure, which has not yet been published. The main contribution is the investigation of control algorithms, hence, WPEAs, for this novel fluid power PTO system design.

First, a description of the physical test setup is given, followed by the main equations forming a non-linear model. Then the optimal torque parameters are calculated and shown with the chosen control cases. Lastly, the WPEAs are created, tested, and implemented on both the simulated model and the test rig. The paper concludes by evaluating the tested control strategies.

2. System Description

The Floating Power Plants concept consists of a floating platform. This platform carries a wind turbine and four wave energy converters. Each wave energy system consists of a wave absorber hinged to the platform, a push rod, a beam, and a main axle connected to a PTO system located in an indoor area (PTO housing). Figure 1 illustrates a single-wave energy converter on which the PTO housing and the rotation points A and B are attached and follow the movement of the floating platform. If one imagines a coordinate system 0, which is attached to the floating platform, the points A and B of each wave energy converter

is fixed in that coordinate system. Moreover, the four-wave energy converters experience the same x , y coordinates for their respective A and B point, but their z coordinate will differ. The four wave energy converters are hence placed equally spaced in the z direction. The absorber of each wave energy converter rotates around point A, which results in a relative movement between each absorber and the platform. Through the push rod, the beam and the main axle, the absorbers motion is transformed to a bidirectional rotation of the main axle, B. Note that the rotation is non-uniform in amplitude and is in the range of ± 20 degrees for the small-scale proof-of-concept wave energy converter.

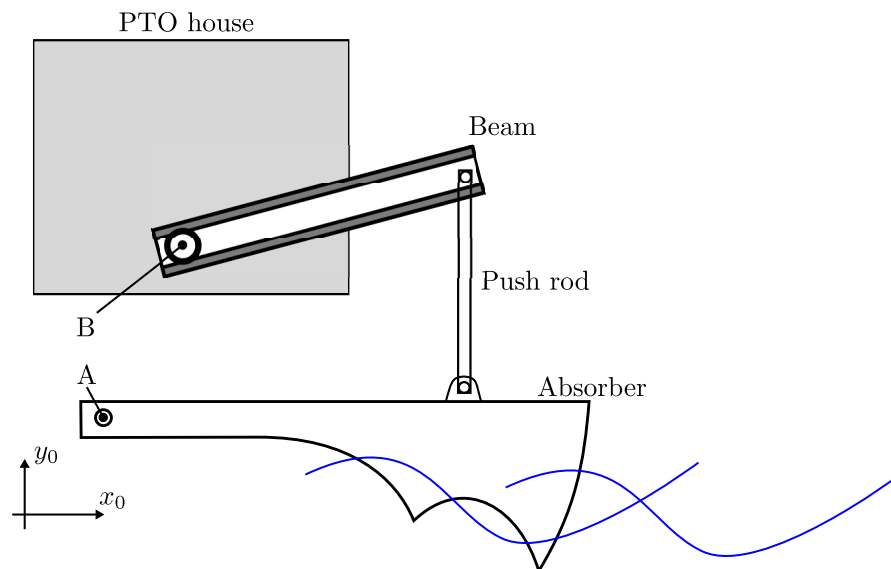


Figure 1. Illustration of the FPP wave energy concept.

The hydraulic PTO system, located in the PTO housing seen in Figure 1, harvests energy from the motion of the main axle, as seen in Figure 2. The main axle rigidly connects to a yoke connecting two differential cylinders, the PTO cylinders ①, to the motion of the main axle and, as such, to the absorber. The PTO cylinders function as a piston pump in which the check valves, ⑥, connect to the in- and outlet. The outlet, the high pressure or system pressure line, ②, is equipped with accumulators, ③, used for smoothing power flow through the hydraulic motor, ④, driving an electrical generator, ⑤. Four on/off valves, ⑦, are installed to allow choosing various pumping areas for the cylinders, changing the displacement flow delivered to the system pressure line for each cylinder stroke. However, varying the cylinder areas connected to system pressure also varies the cylinder force and torque applied on the yoke and the absorber. This torque opposing the absorber motions generates power since power equals torque multiplied angular velocity.

2.1. Physical Test Setup

A small-scale test system is provided by Floating Power Plant A/S [9]. The small scale test system consists of a dry-land absorber emulator system, which drives the scaled PTO system under test. A numerical absorber model, derived in [10], running in real-time, generates the reference for the emulator. Inputs to the numerical model is a wave time-series torque, τ_{ext} , and the real-time measured PTO torque, τ_{pto} , delivered from the tested PTO system. The control concept for the dry test rig is illustrated in Figure 3. The numerical absorber model outputs yoke angle, θ_{yoke} , and angular rate, $\dot{\theta}_{yoke}$, both of which are used as references in the wave cylinder controller. The wave cylinder controller further uses measurements of the system pressures; supply, tank, chamber A and B, p_S , p_T , p_A , p_B in the calculation of valve spool reference, $x_{v,ref}$ for the 4/3 way valve.

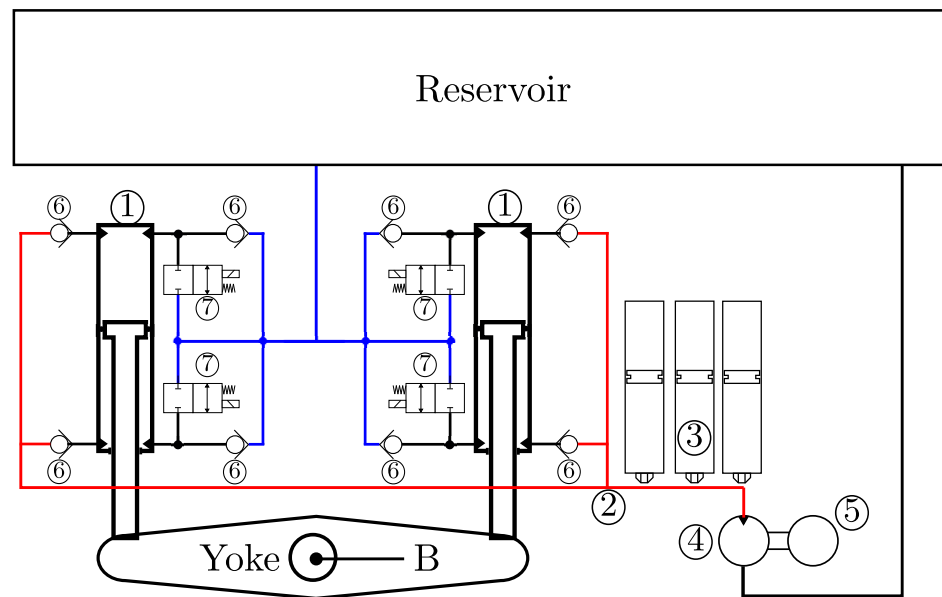


Figure 2. Simple illustration of the power take-off in the PTO housing, note that point B is the same as in Figure 1. Blue and red line colors indicates low and high pressure respectively.

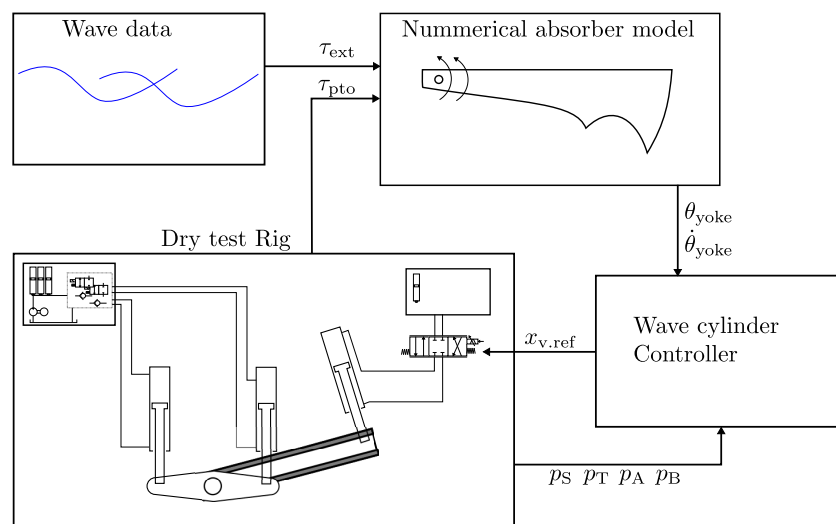


Figure 3. Control and reference concept illustration for the dry test rig.

The absorber emulator system consists of a hydraulic differential cylinder, a proportional valve, and a hydraulic power unit (HPU).

The small-scale PTO system consists of two hydraulic differential cylinders, three piston accumulators, four on/off valves, eight check valves, and a hydraulic motor, as seen in Figure 4. The PTO system is linked with the float emulator system by a shared axle and a beam. Therefore, when the float emulator system runs, the hydraulic cylinders will be compressed and expanded, respectively, when the float emulator moves in a positive and negative direction.

The combined system has three controllable inputs: the proportional valve of the float emulator system, the torque of the electrical generator, and the setting of the four 2/2 directional valves connected to each side of the two cylinders in the PTO system. The PTO test system was initially developed and used to conceptually test and demonstrate Floating Power Plants wave energy technology on a small scale.

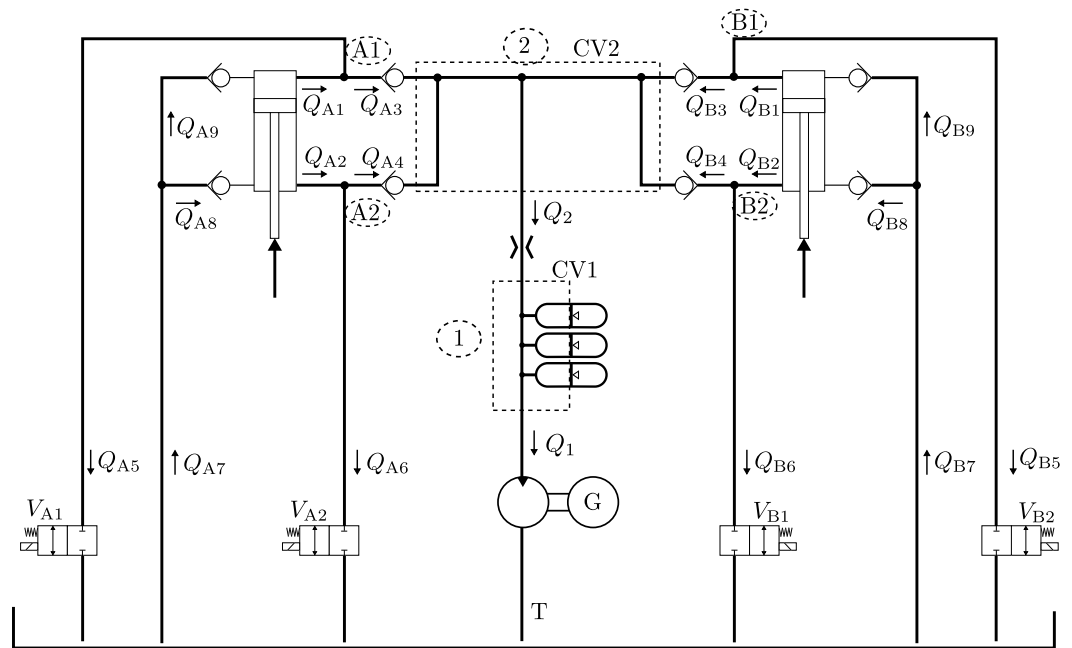


Figure 4. The hydraulic diagram of the PTO system.

2.2. Non-Linear Model

A non-linear model has been created enabling development and test of different control strategies. The model consists of three parts: the mechanical, the absorber emulator, and the PTO system.

The mechanical model centres around an equation of motion based on Newtons Second Law, where the forces F_A , F_B , and F_C are created from the pressures of cylinders A, B, and C, respectively. The gravitational force of the float emulator arm, F_{gC} , viscous and coulomb friction are also modelled with friction coefficients B_{body} and $\tau_{coubody}$, respectively.

$$\ddot{\theta} I_{mech} = -F_C L_{arm} C \cos(\alpha_C) - F_{gC} L_{cm} C \cos(\alpha_{CM}) + F_A L_A C \cos(\theta) - F_B L_B C \cos(\theta) - (B_{body} \dot{\theta} + \tau_{coubody} \text{sign}(\dot{\theta})) \quad (1)$$

The model for the PTO system, as seen in Figure 4, consists of an equation of motion for the hydraulic motor, a continuity equations for each of the control volumes 1 and 2 and for each of the four cylinder chambers, flow equations modelling flow through the valves, and an equation of motion for the piston in each of the accumulators. Firstly the motion of the motor is modelled as:

$$I_m \ddot{\phi} = (p_1 - p_T) D_\omega - B_{md\phi} \dot{\phi} - B_{mpres} (p_1 - p_T) - \tau_{col.m} \text{sgn}(\dot{\phi}) - \tau_{gen} \quad (2)$$

where I_m is the mass inertia of the motor and generator combined, D_ω is the motor displacement, $p_1 - p_T$ is the pressure difference across the motor and τ_{gen} is torque from the electrical generator while $B_{md\phi}$, B_{mpres} , $\tau_{col.m}$ are friction coefficients. Next the continuity equations for all pressure nodes is set up. Here, i signifies the relevant pressure node as marked on Figure 4 as dotted circles, and ΣQ the net flow into the control volume with volume V_i .

$$\dot{p}_i = \frac{\beta}{V_i} (\Sigma Q - (\dot{V}_i)) \quad (3)$$

The flows, Q_j , through check valves and on/off valves as seen on Figure 4 can be described as Equation (4). The on/off valves are either open or closed depending on x_v being 1 or 0, respectively. The check valves are only ever open in one direction, and thus x_v will be 1 or 0 depending on whether p_n or p_m , which are the pressure before and after the valve, are higher.

$$Q_j = \frac{Q_{nom.j}}{\sqrt{p_{nom.j}}} x_v \sqrt{|p_n - p_m|} \text{sgn}(p_n - p_m) \quad (4)$$

The valve flow rating is given by the nominal flow and pressure, $Q_{nom,j}$ and $p_{nom,j}$. Note, that the counter n and m are some specific pressure naming relative to the flow Q_i , where, e.g., Q_{A4} uses p_{A2} and p_2 , see Figure 4.

For the three accumulators, three identical equations of motion can be defined as:

$$m_{acc,k}\ddot{x}_{acc,k} = (p_1 - p_{g,k})A_{acc,k} - F_{fric,acc,k} \text{ for } k = 1, 2, 3 \quad (5)$$

where the counter k reference to each of the three accumulators and m_{acc} is the mass, $A_{acc,k}$ is the piston area in the accumulator, $F_{fric,acc,k}$ is the friction on the piston while $p_{g,k}$ is the gas pressure in said accumulator with piston position $x_{acc,k}$.

3. Optimal PTO Torque

The generator torque and the configuration of the on/off valves are controllable inputs in the PTO system. Since adjusting these inputs will change the torque applied on the absorber from the PTO system (τ_{PTO}), and thereby the amount of energy harvested, an optimal configuration needs to be determined. The optimal configuration will be the one extracting the most energy from each incoming wave. The absorber emulator simulates the actual absorber of the scaled Floating Power Plant wave energy converter in the ocean that is excited by the incoming wave motion. In Figure 5, a free body diagram of the FPP's absorber is given. Note that the hinge point, around which the absorber rotates, is point A in Figure 1 and this point is fixed in the platform coordinate system 0.

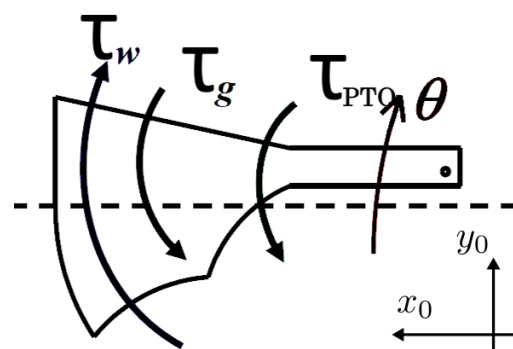


Figure 5. FBD showing the different forces working on the floater.

The different torques in form of the incoming wave torque τ_w , the gravitational torque τ_g , the hydraulic PTO torque τ_{PTO} together results in the absorber's angular displacement θ . The equation of motion for the absorber can be described by an equivalent mass-damper-spring system as in (6). Note that the PTO torque is assumed a linear combination of angular position, velocity, and acceleration as given in (7). With the incoming wave assumed to be a linear wave, the equations become:

$$|M_e|\cos(\omega t + \delta) = \ddot{\theta}(t)(J + m_h(\omega) + m_{PTO}) + \dot{\theta}(t)(c_h(\omega) + c_{PTO}) + \theta(t)(k_h + k_{PTO}) \quad (6)$$

$$\tau_{PTO} = \ddot{\theta}(t)m_{PTO} + \dot{\theta}(t)c_{PTO} + \theta(t)k_{PTO} \quad (7)$$

The absorber's equation of motion is given by the amplitude of the wave excitation torque $|M_e|$ and the incoming wave frequency ω . The acceleration relates to the absorber's inertia J , hydrodynamic mass m_h , and control parameter m_{PTO} . The hydrodynamic damping coefficient c_h and damping control parameter c_{PTO} relates to the floater's velocity and the stiffness coefficients k_h and k_{PTO} relates to the hydrostatic spring constant and control stiffness. It is also relevant to mention that the hydrodynamic coefficients m_h and c_h are frequency dependent on the incoming waves [4,11].

There are different strategies for extracting energy in waves on the ocean. Resistive and reactive control strategies are investigated throughout this paper, and for each control strategy it is relevant to know how much energy the floater is able to absorb, and how much

energy the motor is able to generate, when adjusting the control parameters m_{PTO} , c_{PTO} , and k_{PTO} . Therefore the theoretical control optimum for the current absorber is investigated. This is done by assuming an ideal loss-free PTO system that can apply a continuous PTO torque. In the next sections the resistive control coefficient, c_{PTO} , is firstly investigated to find the optimal value in various regular wave conditions for the current wave absorber. Next the resistive and reactive control coefficients, c_{PTO} and k_{PTO} , are investigated again to find the optimal values for the absorber in regular wave conditions. The optimal control coefficients for resistive and reactive control are hence given in various regular wave conditions, where optimality is when the most energy is harvested, $\int \tau_{pto}(t)\dot{\theta}(t)dt$.

3.1. Resistive Case

The resistive control case is based on only adjusting the control damping coefficient c_{PTO} and setting m_{PTO} and k_{PTO} to zero. This control coefficient is directly related to the instantaneous power that it is possible to harvest through the PTO system and is given by (8) [4].

$$P_a(t) = \tau_{PTO}(t)\dot{\theta}(t) = c_{PTO}\dot{\theta}(t)^2 \quad (8)$$

Integrating the instantaneous power for a period of T and inserting the control parameter c_{PTO} results in an average power expression as in (9) [4].

$$\bar{P}_a = \frac{1}{T} \int_0^T c_{PTO}\dot{\theta}(t)^2 dt \quad (9)$$

This expression can be solved by remembering the assumption of linear waves which has the general motion solutions of (10) where only the real part of the solution is of interest [4].

$$\theta(t) = \text{Re}(A_A e^{i\omega t})\dot{\theta}(t) = \text{Re}(i\omega A_A e^{i\omega t})\ddot{\theta}(t) = \text{Re}(-\omega^2 A_A e^{i\omega t}) \quad (10)$$

Through integration and inserting the harmonic velocity solution into (9) results in the average power expression in (11) [4].

$$\bar{P}_a = \frac{1}{2} |A_A|^2 \omega^2 c_{PTO} \quad (11)$$

The absorber's amplitude can similarly be found from the general solutions to a regular linear wave and by inserting (10) into (6) results in the floater amplitude $|A_A|$ in (12) [4].

$$|A_A| = \frac{|M_e|}{\sqrt{(k_h - \omega^2(J + m_h))^2 + \omega^2(c_h + c_{PTO})^2}} \quad (12)$$

Inserting this expression into the average power of (11), it is possible to find the optimal analytical torque. Adjusting the value of c_{PTO} for each incoming wave with a different frequency it is possible to find the optimal value of c_{PTO} that results in the highest power. In Figure 6, there is a heat map with the wave period in seconds on the x -axis and the changing resistive coefficient c_{PTO} on the y -axis. The changing colours are the average power extracted for each wave period and at a specific value of c_{PTO} . The red curve represents the optimal value of c_{PTO} at a given frequency and thereby the optimal analytical torque for each incoming wave frequency.

The ideal values of c_{PTO} will later be used when calculating the optimal torque reference for the resistive control strategy.

3.2. Reactive Case

It is also possible to expand the analysis of the optimal torque by reconsidering the control parameter k_{PTO} . Instead of setting k_{PTO} to zero, it could be included in the analysis as well, resulting in an optimal reactive torque. The control case being reactive means

that the aim is to align the wave excitation torque with the absorber velocity to achieve resonance and thereby maximise absorber amplitude.

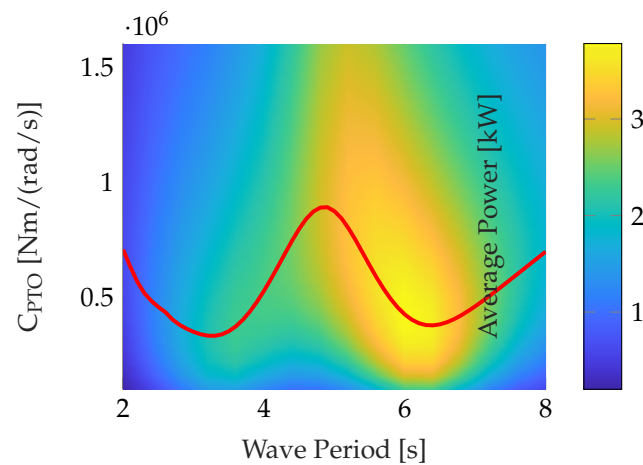


Figure 6. Heat map showing the optimal value of C_{PTO} and the corresponding absorbed power as a function of different wave periods. Wave input: Regular with height of 0.5 m.

Including k_{PTO} and performing the same derivation as in the resistive case results in a floater amplitude expression as in (13) [4].

$$|A_A| = \frac{|M_e|}{\sqrt{(k_h + k_{PTO} - \omega^2(J + m_h))^2 + \omega^2(c_h + c_{PTO})^2}} \quad (13)$$

To achieve resonance between the floater and wave the control parameter k_{PTO} can be adjusted such that it cancels the left denominator expression as in (14) [4].

$$k_h + k_{PTO} - \omega^2(J + m_h) = 0 \quad (14)$$

Fulfilling (14) and inserting (13) into (9) results in an average reactive power expression as in (15) [4].

$$\bar{P}_a = \frac{1}{2} \frac{|M_e|^2 \omega^2 c_{PTO}}{\omega^2 (c_h + c_{PTO})^2} \quad (15)$$

The optimum absorbed power is then found by letting c_{PTO} be equal to the hydrodynamic damping coefficient c_h . This results in the optimal absorbed power through reactive control as in (16) [4].

$$\bar{P}_a = \frac{1}{8} \frac{|M_e|^2}{c_h} \quad (16)$$

Equating the optimal analytical reactive power for a regular wave with constant amplitude and changing wave period and assuming it is possible to adjust the control parameters for any given wave results in the control parameter graphs in Figure 7. The top and bottom graphs illustrate the control parameters c_{PTO} and k_{PTO} that achieve resonance and thereby analytical optimal torque for a given wave period.

These coefficient values are used when implementing the reactive control strategy in the simulations. It should be noticed that implementing k_{PTO} results in the need for external energy. In the project's PTO system, this could come from the accumulators. In the case of supplying external energy, it may conduct extra valve switches which result in higher switching losses.

The optimal values of c_{PTO} and k_{PTO} in Figures 6 and 7 are used to calculate an optimal torque reference when implementing the control cases to the PTO system [4,10,11].

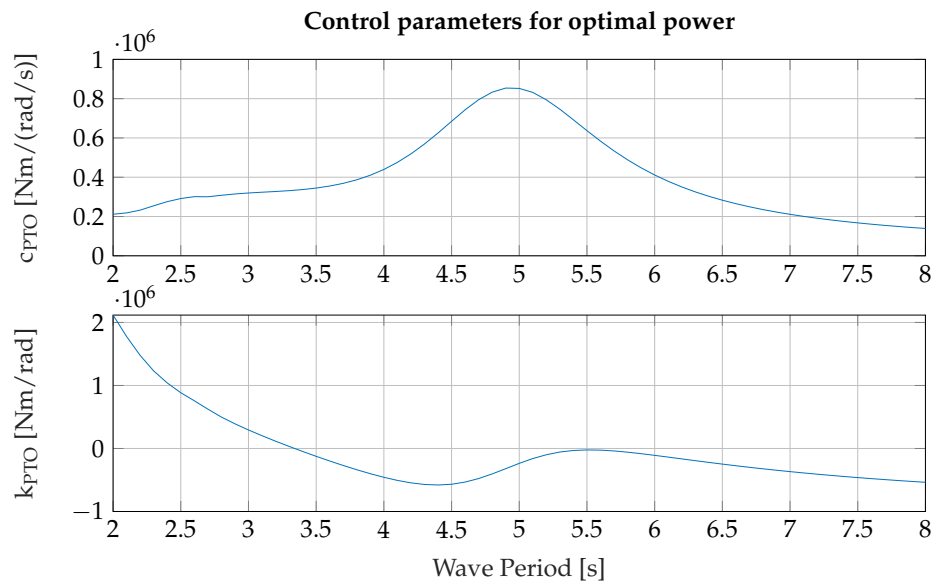


Figure 7. Damping and spring constants to achieve resonance and maximum power at different wave period.

4. Wave Power Extraction Algorithms

In Section 3 it was found that an optimal torque can be constructed for the float at all times in both a resistive and reactive case, as given by, respectively, (17) and (18) [4].

$$\tau_{res.opt} = C_{PTO}\dot{\theta} \tag{17}$$

$$\tau_{reac.opt} = K_{PTO}\theta + C_{PTO}\dot{\theta} \tag{18}$$

These optimal torque references are, however, not realisable for the FPP system that can only change the PTO torque to discrete levels by opening and closing the on/off valves as shown in Figure 4. The WPEA strategies are then given by which valves to open at which times in order to achieve maximum power extraction from the waves to the generator.

4.1. Resistive Case

For resistive implementations multiple methods are presented and investigated:

- All valves closed at all times—reference case.
- Switching only occurs at position endpoints (no velocity).
- Switching can be done continuously throughout the PTO movement.

The PTO torque for the two hydraulic cylinders is described by (19).

$$\tau_{PTO} = L_{PTO}\cos(\theta)((p_{A1}A_{AA} - p_{A2}A_{AB}) - (p_{B1}A_{BA} - p_{B2}A_{BB})) \tag{19}$$

The PTO system can realise three levels of torque in each direction of rotational movement; both cylinders actuated at maximum torque, decoupling the ring chamber for medium torque, and decoupling the bore chamber for low torque. This will effectively change the compressing chamber pressure between high and tank. The possible valve configurations thus become:

	V_{A1}	V_{A2}	V_{B1}	V_{B2}
$V_{config.H+} =$	[0	0	0	0]
$V_{config.H-} =$	[0	0	0	0]
$V_{config.M+} =$	[0	1	0	0]
$V_{config.M-} =$	[0	0	0	1]
$V_{config.L+} =$	[0	0	1	0]
$V_{config.L-} =$	[1	0	0	0]

Where the subscripts H , M , and L indicate high, medium, and low torque, respectively, and where + or – denotes the direction of velocity. Recall that an open valve, 1, means said chamber is connected to the tank.

In the “All Valves Closed” WPEA all on/off valves are closed at all times as a baseline WPEA. This will generate maximal power as long as the waves have a torque larger or equal to the maximum available PTO torque. If the waves become too small, this WPEA will have no way of decreasing the PTO torque to a more appropriate level and will thus stop the motion of the absorber.

The “Endpoint” WPEA is able to switch between all configurations but is only allowed to do so when the piston reaches a velocity of zero which occurs at the positional top and bottom of the cylinder movement. As such, this WPEA is able to adapt the PTO torque to the wave conditions and the ideal torque, but can only do so before the incoming wave, and has to run on the same level throughout the wave. Therefore, this solution can be very effective if the incoming wave is known through predictive control or active wave measurements. The current system, however, does not have this and as such this WPEA will run based on the assumption that the next wave will have the same ideal torque level as the previous one. When the piston meets a velocity of zero, the WPEA will then calculate the ideal torque from the previous wave and set the torque for the next wave at this level.

The “Continuous” WPEA is able to switch levels continuously and as such will, in discrete steps, calculate the ideal torque at all times and set the PTO torque at the closest level. This means that during a wave, the continuous WPEA is able to reach all three levels on the way up in velocity and again on the way down. This WPEA is in theory the one that comes closest to the ideally calculated continuous torque. The theoretical torque delivered by the different WPEAs compared to an optimal reference are illustrated in Figure 8. Note that the optimal is the resistive control with optimal control coefficients and a continuous PTO system.

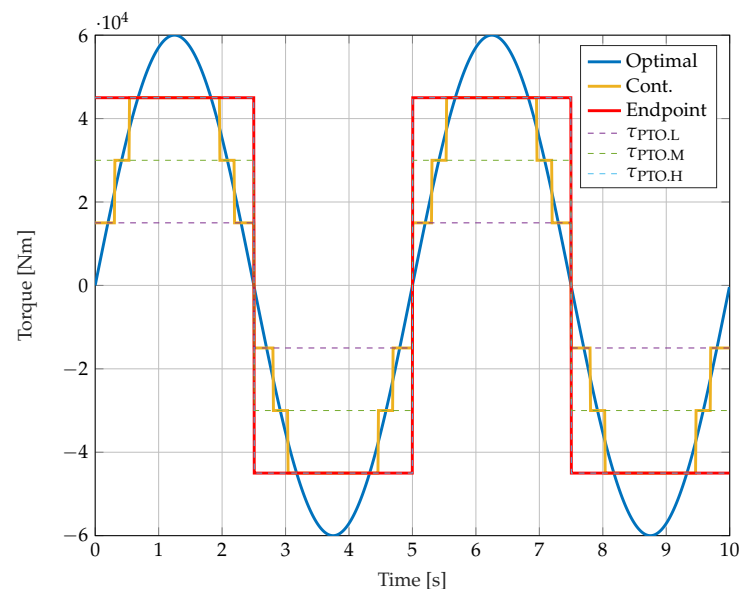


Figure 8. Torque levels for different resistive WPEAs compared to the optimal.

This is an idealised version of the continuous switching, and through the simulation of the mathematical model, it is found that several factors disrupt the tracking of the ideal torque. First, it is found that switching between the medium and low levels in rapid succession is not ideal. When switching from high to medium, the pressure in the ring chamber is dropped to the tank. Then, when switching from the medium to low level, the pressure in the bore chamber is dropped to the tank, and it is desired for the pressure in the ring chamber to become high again. As the ring pressure was just dropped to the tank, there is a moment between medium and low where the pressure in all chambers are

equal to tank pressure, at which point the system produces no torque, before the pressure is built up in the ring chamber again. This creates an unwanted torque drop, and as such, to optimise the continuous switching WPEA, the algorithm is modified to never be able to switch directly between medium and low.

Secondly, it is observed that when the all closed and the endpoint WPEAs switch direction there is a remnant pressure from the previous motion built up in the now-expanding chamber. For example, on the A-cylinder in positive direction, the pressure will be built up in the ring chamber. Then when the endpoint is reached and the direction changes this pressure is still present in the ring chamber before the pressure is built up in the bore chamber. This creates an accelerating effect on the cylinder and makes the system able to achieve high pressure in the retracting chamber faster. This accelerating effect is found to increase the power output of the system as the pressure is usually too slow to increase in order to follow the optimal calculated torque. This effect is not present in the continuous case as the pressure is dropped during the deceleration of the chamber as to follow the ideal torque line. This results in the all closed and the endpoint WPEA being faster at building up pressure than the continuous case and, as such, in order to increase the pressure build-up, the continuous case is modified to always hold the largest level for one-fourth of the wave period before being able to switch continuously as to aid the pressure build-up. This WPEA will be called “Optimised Continuous” for the testing, where it cannot switch between medium and low and where the highest torque level is set for one-fourth of the wave period. The simulated switching patterns for a regular wave with a height of 0.35 m and a period of 5 s can be seen in Figure 9 at steady-state with a 115 bar system pressure.

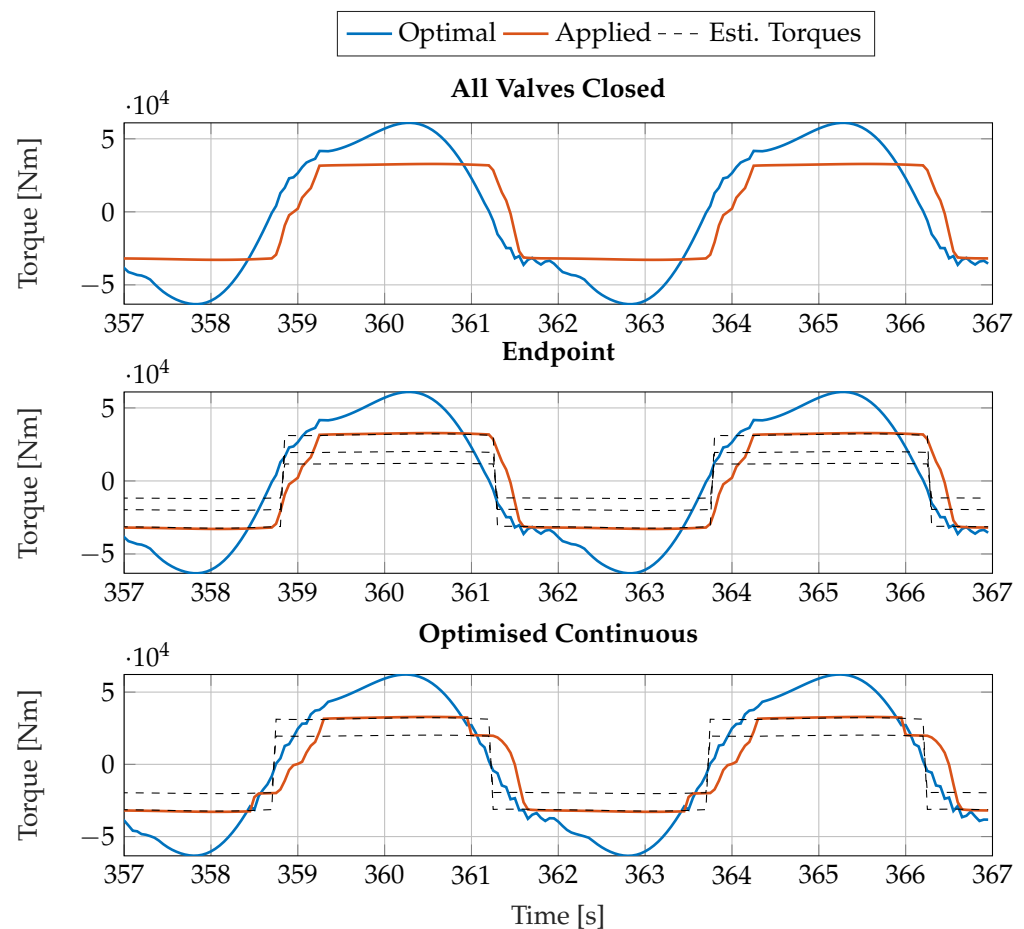


Figure 9. The optimal torque, the applied torque and the estimated possible torques for the three WPEAs at a system pressure of 115 bar during a regular wave with a height of 0.35 m and a period of 5 s.

4.2. Reactive Case

An ideal torque was presented for both a resistive case and a reactive case. In order to realise the reactive control, the system needs to be able to use some of the accumulated energy to assist the movement of the float, to ensure resonance between wave and floater at all frequencies. Therefore, it is proposed to implement a set of high-pressure pathways from the high-pressure common line and back into the chambers of the PTO cylinders. This can be achieved for the Floating Power Plant setup by replacing the check valves, located at nodes A1, A2, B1, and B2 in Figure 4, with a parallel check valve/on-off valve connection.

This configuration allows the system to operate as usual when all the added on/off valves are closed, but also creates the possibility of routing high pressure back into the expanding chambers that would otherwise have fallen to tank pressure. In combination with this, the on/off valves connected to the tank can be opened on the contracting side to reduce the built up pressure, effectively aiding the motion of PTO in correspondence with the wave. This creates the possibility of creating aiding torque that, instead of extracting power from the waves, aids the motion of the waves. In this way, the motion can be aided at strategic times such that the ideal calculated reactive torque of (18) can be achieved. This creates a new set of valve configurations with the added possibility of aiding torque:

	V_{A1}	V_{A2}	V_{A3}	V_{A4}	V_{B1}	V_{B2}	V_{B3}	V_{B4}
$V_{config.H+} =$	[0	0	0	0	0	0	0	0]
$V_{config.M+} =$	[0	0	0	0	0	0	0	1]
$V_{config.L+} =$	[0	0	1	0	0	0	0	0]
$V_{config.aid.H+} =$	[0	1	1	0	1	0	0	1]
$V_{config.aid.M+} =$	[0	0	1	0	1	0	0	1]
$V_{config.aid.L+} =$	[0	1	1	0	0	0	0	1]
$V_{config.0+} =$	[0	0	1	0	0	0	0	1]
$V_{config.H-} =$	[0	0	0	0	0	0	0	0]
$V_{config.M-} =$	[0	0	0	1	0	0	0	0]
$V_{config.L-} =$	[0	0	0	0	0	0	1	0]
$V_{config.aid.H-} =$	[1	0	0	1	0	1	1	0]
$V_{config.aid.M-} =$	[1	0	0	1	0	0	1	0]
$V_{config.aid.L-} =$	[0	0	0	1	0	1	1	0]
$V_{config.0-} =$	[0	0	0	1	0	0	1	0]

Where V_{A3} and V_{B3} opens high pressure to the bore chambers and V_{A4} and V_{B4} opens high pressure to the ring chambers. As in the continuous case, the low level is not utilised because of the brief pressure drop during switching. As the reactive case does not switch at endpoints but instead switches during the movement, unless operating at a resonance frequency, the switching pattern during simulation is illustrated in Figure 10 for a 6.5 s period operating at 115 bar system pressure.

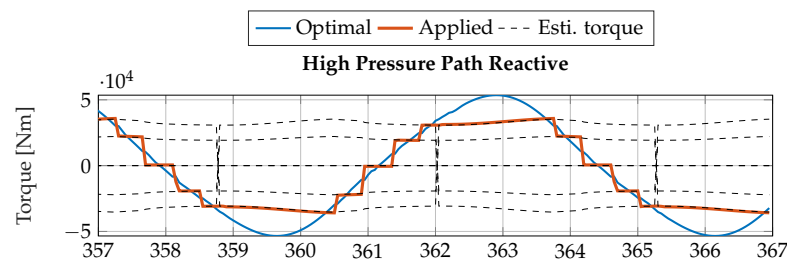


Figure 10. Actual PTO torque and ideal PTO torque for the high-pressure path-aided reactive strategy measured with a system pressure of ~115 bar. Wave input: Regular with a height of 0.35 m. and a period of 6.5 s.

Here it is seen from the estimated torque levels that the PTO torque for the positive direction, between 362 and 365 s, is working in opposition to the wave torque at most of the stroke length but aids the wave torque in the end, to correct the phase difference. The further from the resonance frequency that the wave torque is, the more of the stroke length the WPEA needs to apply aiding torque. As such, the reactive WPEA performance becomes very sensitive to the wave frequency. The reactive WPEA for an irregular wave also needs to correctly know the frequency of the current wave in order to calculate the correct K_c cancellation and as such would also be expected to have diminished performance on an irregular wave, unless predictive control or active measurements are implemented.

4.3. Generator Torque Strategy

Through simulations, it has been shown that at each frequency there are specific system pressures at which the WPEA generates more energy. If the pressure in the cylinders is too low, the WPEA does not have the possibility of following the ideal torque correctly, but if the generator torque becomes too high, the motor will never start spinning as the leakage pathways become the paths of least resistance. If power over pressure graphs, such as Figure 11, are observed, it becomes clear that for all wave conditions there are unique optimal generator torques.

To determine an expression of this torque the hydraulic motor equations are observed.

$$I_m \ddot{\phi} = \Delta p D_\omega - \underbrace{B_{md\phi} \dot{\phi} - B_{mpres} \Delta p - \tau_{col.m}}_{\text{Loss}} - \tau_{gen} \quad (20)$$

$$Q_1 = \dot{\phi} D_\omega + \underbrace{C_{le.m} \Delta p}_{\text{Loss}} \quad (21)$$

where Δp denotes the pressure differential over the hydraulic motor (system pressure), and the friction is modelled as having a static coulomb friction part, a motor velocity-dependent part, and a pressure-dependent part.

To obtain optimal energy, the losses must be reduced. The motor friction loss increases with the pressure and the velocity in (20). The pressure, however, is also included in the torque generated from the displaced liquid and is needed for the PTO to absorb the wave power optimally and thus needs to be kept high in order to produce energy. The velocity, though, can be reduced to decrease friction losses. If the velocity is reduced to zero in (20), the equation can be rewritten as describing the minimal torque needed for the system to have a velocity of zero if observed at a steady velocity (no acceleration). Any torques above this will stop the motor and thus applying a torque slightly lower than this value becomes the maximum torque at which the motor can still rotate.

$$\tau_{gen} = \Delta p D_\omega - B_{md\phi} \dot{\phi} - B_{mpres} \Delta p - \tau_{col.m} \quad (22)$$

Which can be simplified to a generator torque control expression.

$$\tau_{gen} = \Delta p (D_\omega - B_{mpres}) - \tau_{col.m} \quad (23)$$

This observation indicates that the optimal operation torque-to-velocity ratio for the motor becomes maximal torque with minimum motor velocity. Simulations reveal the same through creating a feedback loop from the velocity to set the torque. With PI control implemented, it is possible to, by controlling the motor torque, follow a motor velocity reference to test the performance at different velocities. This test indeed shows that optimal power is generated at the lower velocities, between 500 and 1000 rpm, depending on wave frequency and height.

Equation (23) does not, however, take leakage into account. The leakage over the motor, described in (21), increases with the pressure, meaning that it is desired to increase the torque to reduce the influence of friction but not increase it too much so as to create too

much leakage. Larger torques and thus larger pressures also decrease the motion of the float. Therefore the optimal torque for the motor must be found as a compromise between friction and leakage/damping. As the leakage of this system is so low with a motor friction coefficient of 2.5×10^{-12} it makes sense that the optimal power would prioritise lowering the velocity to reduce friction. Additionally, increasing the generator torque and thus the system pressure also makes the PTO able to follow the calculated ideal torque better, as it achieves higher available torque levels with the increasing system pressure.

To test this hypothesis, the constant multiplier ($D_\omega - B_{mpres}$) of (23) is swept for variations to both sides on the all valves closed WPEA and it is found that the constant needs to be decreased a bit from the calculated version to make the motor spin. The sweep can be seen in Figure 11 compared to applying a constant motor torque for the all closed WPEA.

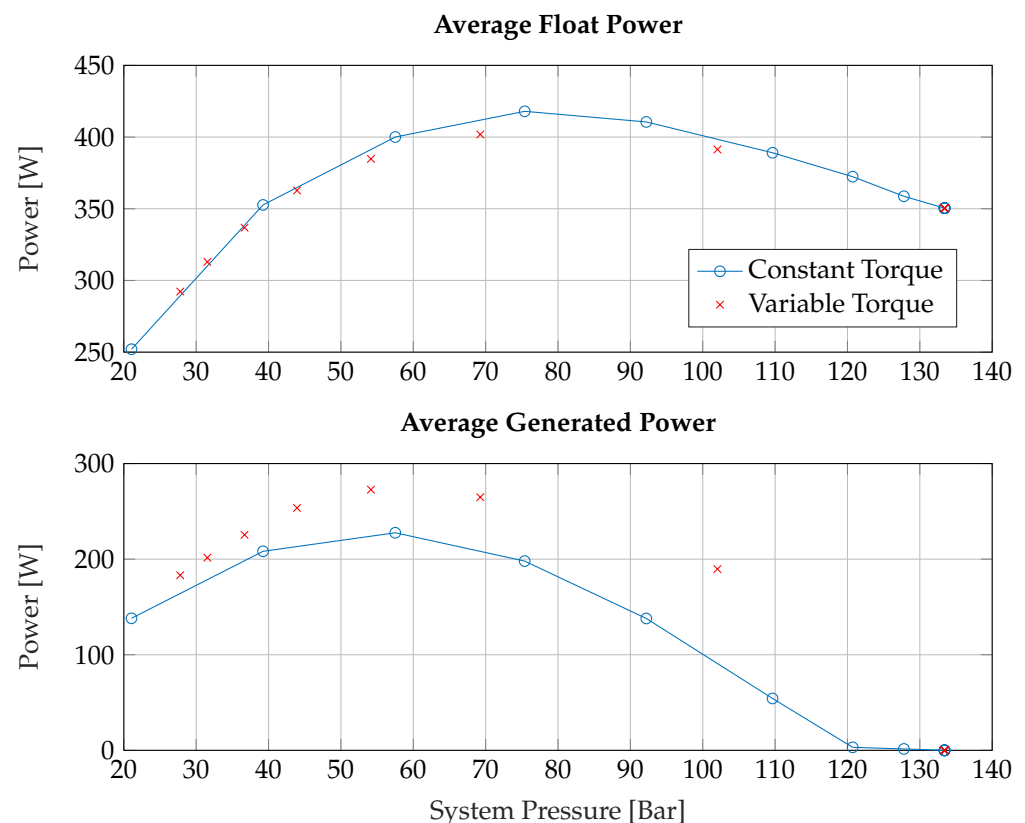


Figure 11. Sweep of motor torque control constants marked in red. Wave input: Irregular Wave.

Where absorber power is the power applied upon the absorber, while generated power is the mechanical power generated by the hydraulic motor onto the generator.

The absorbed power is a bit lower for this generator torque strategy, but the generated power experiences a significant increase. This most likely comes from the fact that the motor is able to run and generate power at all times, where, with a constant torque, it can only produce power when the waves are large enough to build up the pressure in correspondence with the torque level. With the pressure-dependent torque level, the torque will be determined as a function of the pressure such that the motor always runs at a low velocity. As this optimises the generator power, the optimal value is interpolated from the sweep and used for future simulations.

5. WPEA Performance

Four different WPEA strategies have been presented. To evaluate the optimal strategy, the system is simulated on irregular waves and for a frequency sweep to determine the

optimal performance on actual waves and to examine the reactive WPEA performance in regards to the resistive cases at different frequencies.

The average absorbed and generated power for the different WPEAs both using constant and pressure-dependent motor torque can be observed in Figure 12.

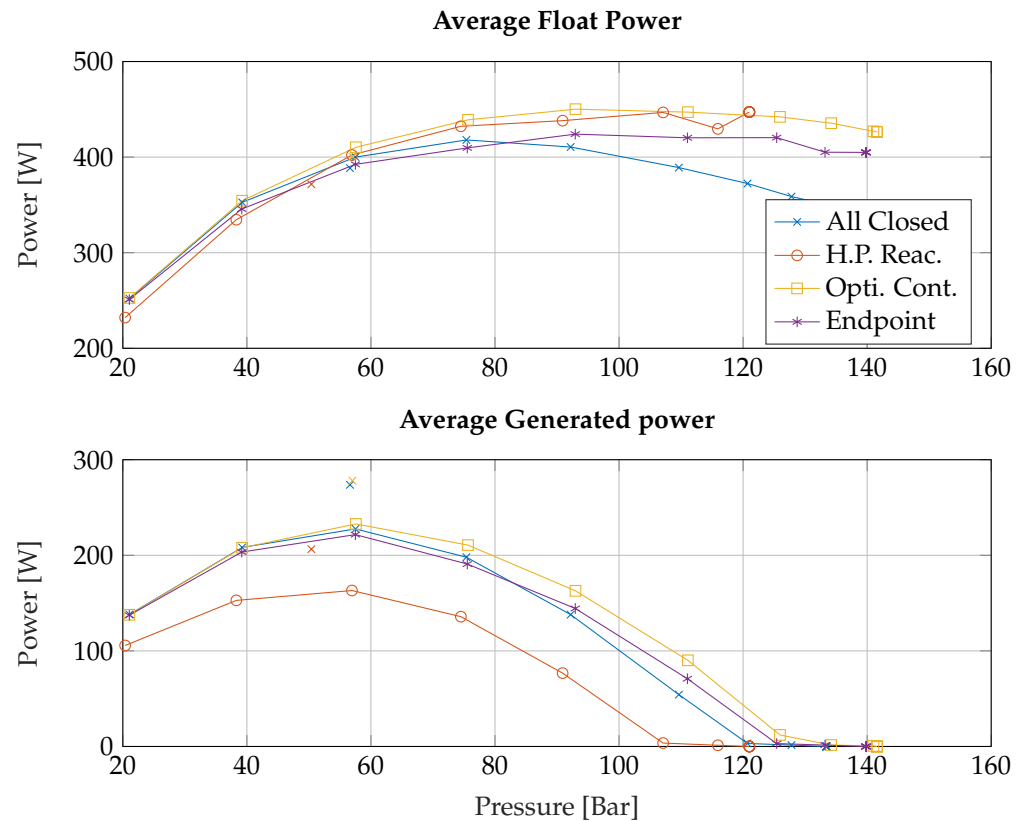


Figure 12. Average power over different system pressures with x-marked optimal motor torque control algorithm. Wave input: Irregular Wave.

Where the pressure-dependent torque performances have been marked in x's in the colour corresponding to the applied WPEA. By implementing the pressure-dependent torque control strategy, it is found that the generated power can be increased by approximately 22% for all WPEAs on the irregular wave.

It can be concluded that for the irregular wave, the best-performing WPEA is the optimised continuous strategy producing ~20 W more than all valves closed at optimum, at a system pressure of 58 bar with the motor torque control. As expected, the endpoint WPEA and the reactive WPEA performs suboptimally on the irregular wave where the frequency and wave height have to be estimated based on the previous wave. If the system is instead observed on a regular wave, where the frequency and wave height is known for all waves, the performance of these strategies is increased. This is shown in Figure 13 where a frequency sweep on regular waves was conducted for periods 2–8.5 s with a wave height of 0.35 m and with generator torque control implemented.

Here, the reactive control WPEA performs significantly better but still falls short for generated power at all periods except for 6.5 s, even though the absorber power has been increased at most periods. This discrepancy between absorber power and generated power comes from the fact that the reactive case needs to use some of the available power to actuate the pistons and the fact that valve and switching losses are increased. So, even though the reactive case amplifies the power of the absorber, not all of this power becomes available at the generator. In this case, the reactive WPEA needs to operate at frequencies where low-power corrections to the phase can significantly increase the extracted power. When operating at the resonance periods, which were found to be located at 3.3 and 5.5 s,

there is nothing for the reactive element to correct, and when operating too far from the resonance periods it takes too much energy to correct the phase. For example, at a period of 8 s, it is observed in the simulation that the WPEA expends as much torque to correct the phase at the end of the movement as it loads in the start, resulting in a net power gain of 0.

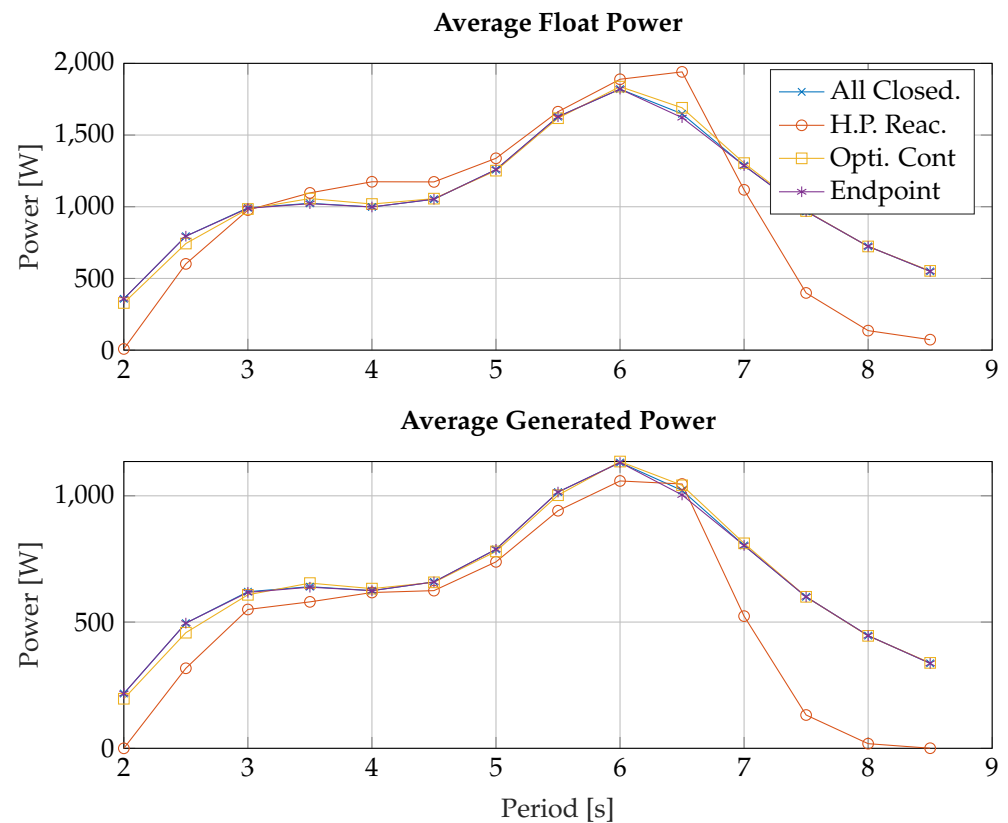


Figure 13. Frequency sweep comparison of resistive WPEAs versus reactive with pressure-dependent generator control. Wave input: regular wave of 0.35 m at varying periods.

The resistive cases behave similarly for all frequencies, with the optimised continuous and the endpoint WPEAs being slightly better. As the endpoint WPEA does not work optimally on irregular waves without predictive elements, the optimised continuous WPEA is concluded to be the best-performing WPEA.

To verify this, the resistive control strategy is implemented on the test rig. As the reactive control strategy requires a physical change, this will not be implemented. The results of the implementation are shown in Figure 14 for optimised continuous, endpoint, and all valve-closed WPEA on an irregular wave. Due to two limitations of the test rig, a motor speed limit of 4000 rpm, and a pressure limit at the system pressure of 150 bar, only the span 4 Nm to 7.5 Nm are tested.

By comparing the simulated average power, Figure 12, with the tested average power, Figure 14, it can be seen that both average absorbed and generated power differ. Part of this deviation is likely due to an inaccuracy between the non-linear model and the test rig where the motor velocity and the system pressure at the motor both deviated. However, the tendency is the same for both simulation and the real test, where maximum absorber power is produced by continuous control and endpoint control becomes better than all closed around 80–90 bar system pressure. A significant difference is that at a system pressure above 120 bar, the endpoint WPEA is now generating more generated power than continuous control. This could perhaps be explained by the model not being accurate enough, so the low torque level which was removed in optimised continuous control now needs to be used regularly.

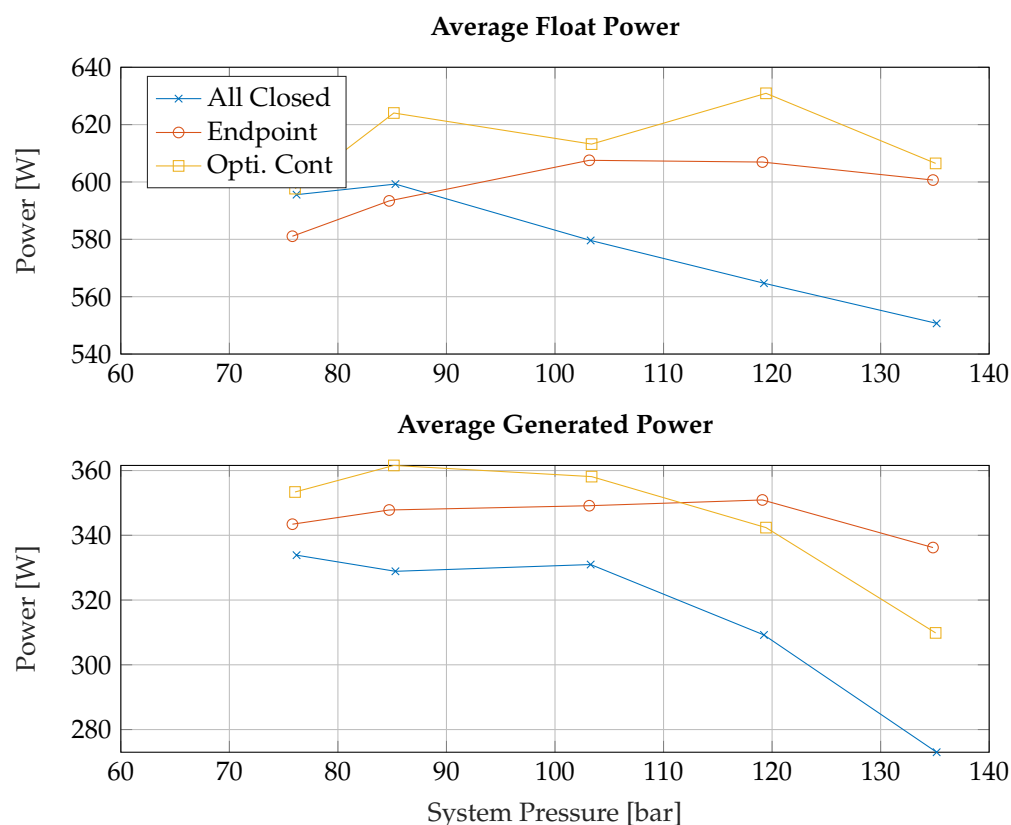


Figure 14. Measurements of absorbed and Generator power as a function of systems pressure using different WPEAs. Wave input: Irregular Wave.

6. Discussion

Based on the results presented, it is seen that the control of the generator used in the Discrete Displacement Cylinder-based PTO system has great influence on the harvested energy. In prior studies on, e.g., the Wavestar concept, the generator was controlled to hold a constant pressure level. This study shows that it is better to control the generator torque based on the actual pressure difference, allowing for pressure variation rather than seeking a control pressure. Furthermore, the studies did not show improvements when implying reactive control, which however has been the case for other point absorber-type WECs. This may be due to the special absorber shape employed by Floating Power Plant and the discrete nature of the applicable PTO torque.

7. Conclusions

In conclusion, of all the wave power extraction algorithms that were tested, a continuously switching resistive algorithm performed the best, evaluated at power output when taking its adaptability to sea conditions into account. Implementing high-pressure pathways to the cylinders and performing reactive control was found not to increase the energy in a bandwidth large enough to become advantageous overall. Both endpoint switching and reactive control can, however, stand to gain increased performance if the incoming wave is known through predictive control or active wave measurements. It would therefore be very interesting to investigate some predictive control algorithms taking wave forecast into account.

Most importantly, one may conclude that a significant power increase is possible by implementing a pressure-dependent motor torque strategy instead of applying constant torque at the hydraulic motor. It is therefore very important to include the generator control in future investigations of PTO control for this type of PTO system.

As these findings are the first published for the current WEC PTO system, they will serve as baseline for future studies on control strategies for the Floating Power Plant technology. Compared to other studies, two interesting findings are seen; firstly, that reactive WPEAs do not improve energy production, which has been the case for other systems moving in a similar manner though with other PTO systems and absorbers; secondly, that the generator for the DDC system should not be controlled to give a constant system pressure level.

Author Contributions: Investigation, N.E.A., J.B.M., M.G.C., C.C., C.-E.H. and A.L.L.; Project administration, A.H.H.; Supervision, A.H.H.; Writing—original draft, N.E.A., J.B.M., M.G.C., C.C., C.-E.H. and A.L.L.; Writing—review & editing, N.F.E. and A.H.H. All authors have read and agreed to the published version of the manuscript.

Funding: Part of the work was supported by the Danish Energy Technology Development and Demonstration Program, under grant agreement 64020-2040.

Conflicts of Interest: N.F.E. is an employee of Floating Power Plant, and has a financial interest in the commercialisation of the company's wave technology.

References

1. Mørk, G.; Barstow, S.; Kabuth, A.K.; Pontes, M.T. Assessing the Global Wave Energy Potential. In Proceedings of the 29th International Conference on Ocean, Offshore Mechanics and Arctic Engineering, Shanghai, China, 6–11 June 2010; pp. 7–8.
2. e Melo, A.B. *Annual Report—An Overview of Ocean Energy Activities*. *Ocean Energy Systems*; The Executive Committee of Ocean Energy Systems: Lisbon, Portugal, 2020.
3. Drew, B.; Plummer, A.R.; Sahinkaya, M.N. A review of Wave Energy Converter Technology. *Proc. Inst. Mech. Eng. Part A J. Power Energy* **2016**, *223*, 887–902. [[CrossRef](#)]
4. Hansen, R.H. *Design and Control of the Power Take-Off System for a Wave Energy Converter with Multiple Absorbers*; Department of Energy Technology, Aalborg University: Aalborg, Denmark, 2013.
5. Lin, Y.; Bao, J.; Liu, H.; Li, W.; Tu, L.; Zhang, D. Review of hydraulic transmission technologies for wave power generation. *Renew. Sustain. Energy Rev.* **2015**, *50*, 194–203. [[CrossRef](#)]
6. Hansen, R.H.; Kramer, M.M.; Vidal, E. Discrete Displacement Hydraulic Power Take-Off System for the Wavestar Wave Energy Converter. *Energies* **2013**, *6*, 4001–4044. [[CrossRef](#)]
7. Hansen, A.H.; Asmussen, M.F.; Bech, M.M. Hardware-in-the-Loop Validation of Model Predictive Control of a Discrete Fluid Power Take-Off System for Wave Energy Converters. *Energies* **2019**, *12*, 3668. [[CrossRef](#)]
8. Maria-Arenas, A.; Garrido, A.J.; Rusu, E.; Garrido, I. Control Strategies Applied to Wave Energy Converters: State of the Art. *Energies* **2019**, *12*, 3115. [[CrossRef](#)]
9. Floating Power Plant. 2021. Available online: <https://www.floatingpowerplant.com/> (accessed on 29 November 2021).
10. Nielsen, S.R.K.; Sichani, M.T.; Kramer, M.M.; Kofoed, J.P. Optimal control of nonlinear wave energy point converters. *Ocean Eng.* **2013**, *72*, 176–187. [[CrossRef](#)]
11. Pecher, A.; Kofoed, J.P. *Handbook of Ocean Wave Energy*; Springer: Cham, Switzerland, 2017; ISBN 978-3-319-81990-7.